Developmental and oncogenic programs in H3K27M gliomas dissected by single-cell RNA-seq

Published in final edited form as:

Science. 2018 April 20; 360(6386): 331–335. doi:10.1126/science.aao4750.

Developmental and oncogenic programs in H3K27M gliomas dissected by single-cell RNA-seq

Mariella G. Filbin[1,2,3,4,5,*], **Itay Tirosh**[3,4,6,*], **Volker Hovestadt**[1,3,4,*], **McKenzie L. Shaw**[1,3,4], **Leah E. Escalante**[1,3,4], **Nathan D. Mathewson**[7], **Cyril Neftel**[1,3,4,8], **Nelli Frank**[9], **Kristine Pelton**[10], **Christine M. Hebert**[1,3,4], **Christine Haberler**[11], **Keren Yizhak**[4], **Johannes Gojo**[5], **Kristof Egervari**[1], **Christopher Mount**[12], **Peter van Galen**[1,3,4], **Dennis M. Bonal**[13], **Quang-De Nguyen**[13], **Alexander Beck**[1], **Claire Sinai**[2,10], **Thomas Czech**[14], **Christian Dorfer**[14], **Liliana Goumnerova**[2], **Cinzia Lavarino**[15], **Angel M. Carcaboso**[15], **Jaume Mora**[15], **Ravindra Mylvaganam**[1], **Christina C. Luo**[1], **Andreas Peyrl**[5], **Mara Popović**[16], **Amedeo Azizi**[5], **Tracy T. Batchelor**[17], **Matthew P. Frosch**[1], **Maria Martinez-Lage**[1], **Mark W. Kieran**[2], **Pratiti Bandopadhayay**[2,4], **Rameen Beroukhim**[4,18], **Gerhard Fritsch**[9], **Gad Getz**[1,4], **Orit Rozenblatt-Rosen**[3,4], **Kai W. Wucherpfennig**[7], **David N. Louis**[1], **Michelle Monje**[12], **Irene Slavc**[5], **Keith L. Ligon**[2,4,10], **Todd R. Golub**[2,4], **Aviv Regev**[3,4,19,†,‡], **Bradley E. Bernstein**[1,3,4,†,‡], and **Mario L. Suvà**[1,3,4,†,‡]

[1]Department of Pathology and Center for Cancer Research, Massachusetts General Hospital and Harvard Medical School, Boston, MA 02114, USA. [2]Department of Pediatric Oncology, Dana-

[†]Corresponding author. suva.mario@mgh.harvard.edu (M.L.S.); bernstein.bradley@mgh.harvard.edu (B.E.B.); aregev@broadinstitute.org (A.R.).
[*]These authors contributed equally to this work.
[‡]These authors contributed equally to this work.

Author contributions: M.G.F., I.T., V.H., B.E.B., A.R., and M.L.Su. conceived the project and designed the study. M.G.F. collected and processed tumor samples, performed all cell culture assays, and planned mouse studies. I.T. and V.H. performed all computational analyses. M.L.Sh., L.E.E., N.D.M., C.N., N.F., K.P., C.M.H., C.H., J.G., K.E., A.B., C.S., T.C., C.D., L.G., C.L., A.M.C., J.M., A.P., M.P., A.A., T.T.B., M.W.K., G.F., and I.S. helped with collecting tumors and generating single-cell sequencing data. N.D.M. helped with CRISPR experiments. R.M. and C.C.L. provided flow cytometry expertise. M.G.F., V.H., and P.V.G. designed and performed targeted sequencing experiments. K.Y., G.G., P.B., and R.B. provided support for genomic and genetic analyses. M.L.Sh. performed in situ hybridization experiments. M.P.F. and M.M.-L. provided samples for in situ hybridization experiments. C.M. and M.M. developed normal human cell cultures used in the study. D.M.B. and Q.-D.N. performed in vivo mouse studies. K.W.W., O.R.R., D.N.L., I.S., K.L.L., and T.R.G. provided experimental and analytical support. M.G.F., I.T, V.H., A.R., B.E.B., and M.L.Su. interpreted results and wrote and edited the manuscript with feedback from all authors.

Competing interests: B.E.B. is an advisor and equity holder for Fulcrum Therapeutics, 1CellBio, and HiFiBio. A.R. is a scientific advisory board member for ThermoFisher Scientific, Syros Pharmaceuticals, and Driver Group. M.G.F., I.T., V.H., A.R., B.B., and M.L.Su. are co-inventors on a U.S. provisional patent application (U.S. 62/585,468) relating to advances described in this manuscript filed by the Broad Institute, MIT, and MGH. G.G. has patent applications on tools for cancer genome analysis. All other authors have no competing interests.

Data and materials availability: Data generated for this study are available through the Gene Expression Omnibus (GEO, accession no. GSE102130) or the Broad Institute Single-Cell Portal (https://portals.broadinstitute.org/single_cell/study/single-cell-analysis-in-pediatric-midline-gliomas-with-histone-h3k27m-mutation). All other data are available in the manuscript or the supplementary materials.

SUPPLEMENTARY MATERIALS
www.sciencemag.org/content/360/6386/331/suppl/DC1
Material and Methods
Figs. S1 to S19
Tables S1 to S8
References (*16–27*)

Farber Boston Children's Cancer and Blood Disorders Center, Boston, MA 02215, USA. [3]Klarman Cell Observatory, Broad Institute of Harvard and Massachussetts Institute of Technology (MIT), Cambridge, MA 02142, USA. [4]Broad Institute of Harvard and MIT, Cambridge, MA 02142, USA. [5]Department of Pediatrics and Adolescent Medicine, Medical University of Vienna, Vienna, Austria. [6]Department of Molecular Cell Biology, Weizmann Institute of Science, Rehovot 7610001, Israel. [7]Department of Cancer Immunology and Virology, Department of Microbiology and Immunobiology, Department of Neurology, Dana-Farber Cancer Institute and Harvard Medical School, Boston, MA 02215, USA. [8]Institute of Pathology, Faculty of Biology and Medicine, Centre Hospitalier Universitaire Vaudois, 1011 Lausanne, Switzerland. [9]Children's Cancer Research Institute (CCRI), St. Anna Kinderspital, Medical University of Vienna, Vienna, Austria. [10]Department of Oncologic Pathology, Brigham and Women's Hospital, Boston Children's Hospital, Dana-Farber Cancer Institute, Boston, MA 02215, USA. [11]Institute of Neurology, Medical University of Vienna, Vienna, Austria. [12]Departments of Neurology, Neurosurgery, Pediatrics, and Pathology, Stanford University School of Medicine, Stanford, CA 94305, USA. [13]Center for Biomedical Imaging in Oncology, Lurie Family Imaging Center, Dana-Farber Cancer Institute, Boston, MA 02215, USA. [14]Department of Neurosurgery, Medical University of Vienna, Vienna, Austria. [15]Developmental Tumor Biology Laboratory, Hospital Sant Joan de Déu, Esplugues de Llobregat, 08950 Barcelona, Spain. [16]Institute of Pathology, Faculty of Medicine, University of Ljubljana, Ljubljana, Slovenia. [17]Departments of Neurology and Radiation Oncology, Division of Hematology/Oncology, Massachusetts General Hospital Cancer Center, Harvard Medical School, Boston, USA. [18]Departments of Cancer Biology and Medical Oncology, Dana-Farber Cancer Institute, and Department of Medicine, Brigham and Women's Hospital and Harvard Medical School, Boston, MA 02215, USA. [19]Department of Biology, Koch Institute for Integrative Cancer Research, Howard Hughes Medical Institute, MIT, Cambridge, MA 02139, USA.

Abstract

Gliomas with histone H3 lysine27-to-methionine mutations (H3K27M-glioma) arise primarily in the midline of the central nervous system of young children, suggesting a cooperation between genetics and cellular context in tumorigenesis. Although the genetics of H3K27M-glioma are well characterized, their cellular architecture remains uncharted. We performed single-cell RNA sequencing in 3321 cells from six primary H3K27M-glioma and matched models. We found that H3K27M-glioma primarily contain cells that resemble oligodendrocyte precursor cells (OPC-like), whereas more differentiated malignant cells are a minority. OPC-like cells exhibit greater proliferation and tumor-propagating potential than their more differentiated counterparts and are at least in part sustained by *PDGFRA* signaling. Our study characterizes oncogenic and developmental programs in H3K27M-glioma at single-cell resolution and across genetic subclones, suggesting potential therapeutic targets in this disease.

Diffuse midline gliomas with histone H3 lysine27-to-methionine mutations (H3K27M-glioma) are uniformly fatal malignancies (1). They are both spatially and temporally restricted, occurring in midline structures of the brain with peak incidence at 6 to 9 years of age. These patterns suggest that a particular cell type, potentially undergoing rapid expansion at this stage, is susceptible to transformation by H3K27M. Experimental models

suggest that neural precursor cells (NPCs) can be transformed in vitro by H3K27M, in combination with *TP53* mutation and *PDGFRA* overexpression (2).H3K27M suppresses EZH2, the catalytic subunit of Polycomb Repressive Complex 2 (PRC2), compromising epigenetic repression and potentially affecting cellular differentiation (1–3). In patient samples, little is known about the developmental cell states present or how they cooperate with H3K27M for tumorigenesis. Single-cell RNA sequencing (scRNA-seq) can help address such questions by characterizing cancer cell states, their proliferative signatures, and their similarity to normal or other malignant cell types. scRNA-seq also helps relate single cell states to genetics through inferred chromosomal copy number variations (CNVs) or mutation detection in expressed transcripts (4–6).

We obtained fresh tissue from diagnostic biopsies of six H3K27M-glioma (table S1 and fig. S1). Each sample was dissociated into single cells, flow sorted, and profiled by means of full-length scRNA-seq (fig. S2) (7, 8). We retained 2458 cells that passed quality controls (8) for downstream analyses (table S2). The cells' profiles group primarily by tumor of origin (Fig. 1A and fig. S3), but two clusters contain cells from multiple tumors, expressing markers of either microglia (such as *CD14, CX3CR1*, and *AIF1*) or oligodendrocytes (such as *MBP* and *PLP1*) (Fig. 1, A and B), suggesting that they are nonmalignant cells. Accordingly, in presumed malignant cells only, we detected evidence for cancer-specific aberrations—point mutations and/or CNVs (4–6)—in 93.7% of cells in five of the six tumors (Fig. 1, C and D, and figs. S4 to S7). Thirty-four percent (833 of 2458) of the cells had H3K27M mutations in scRNA-seq reads mapping to *H3F3A* or *HIST1H3B* (Fig. 1D and fig. S7) only detected in presumed malignant cells; other point mutations from whole-genome sequencing (WGS)/whole-exome sequencing (WES) (tables S1 and S2) were also detected only in presumed malignant cells (Fig. 1D and fig. S7) (8). Analyzing a seventh tumor (MUV17) with *H3F3A*-specific primers in the scRNA-seq protocol confirmed H3K27M in 97% of the presumed malignant cells (fig. S8) (8).

Next, we compared malignant cell transcriptomes across different glioma types, including H3K27M-glioma, isocitrate dehydrogenase (IDH)–mutant oligodendroglioma (IDH-O), IDH-mutant astrocytoma (IDH-A), and IDH–wild-type glioblastoma (GBM) (fig. S9A and tables S3 and S4) (5, 6, 9). Many genes were up-regulated in H3K27M-glioma versus other tumors ($n = 182$ genes), but few were down-regulated ($n = 12$ genes), which is consistent with H3K27M blocking repression by PRC2 (fig. S9, B to D). Accordingly, H3K27M–up-regulated genes are enriched for PRC2 target genes ($P < 0.0001$, hypergeometric test) (fig. S9E) (10, 11). The PRC1 subunit *BMI1* was up-regulated in H3K27M-glioma, possibly representing a compensatory mechanism for PRC2 suppression. Suppression of *BMI1* by means of CRISPR knockout or its pharmacological inhibition reduced viability of H3K27M glioma cells, relative to treatment controls and non-H3K27M glioma lines (fig. S10) (12).

We next assessed patterns of intratumor heterogeneity and distinguished subpopulations of malignant cells within H3K27M-glioma. We identified four programs (P1 to P4) that were consistently observed as variable within tumors and across computational methods (8): cell cycle (such as *PCNA* and *CDK1*), astrocytic differentiation (AC-like) (such as *GFAP* and *APOE*), oligodendrocytic differentiation (OC-like) (such as *MBP* and *PLP1*), and OPC-like

programs (such as *PDGFRA* and *CSPG4*) (Fig. 2, A and B; figs. S11 and S12; and table S5) (13, 14).

Scoring each cell for these expression programs highlighted a putative developmental hierarchy, in which proliferation is largely restricted to OPC-like cells that presumably both self-renew and give rise to the OC-like and AC-like cells (Fig. 2C). The relative fraction of cells in each compartment (OPC-like, AC-like, and OC-like) varied between tumors, but OPC-like cells were consistently the most prevalent (fig. S13). We validated this cellular composition with RNA in situ hybridization (ISH) of seven tumor specimens (table S4), using markers for OPC-like, AC-like, and cycling cells (*PDGFRA, APOE*, and *Ki-67*, respectively) (Fig. 2D and fig. S13). Analysis of normal brain cell types indicated that PRC2 targets are highly expressed by OPCs and lowly expressed by OCs ($P < 0.05$, Student's t test) (fig. S14 and table S6). Thus, OPC differentiation into OC may require the repressive activity of PRC2 and may be hindered by PRC2 inactivation through H3K27M, which may result in accumulation of self-renewing OPC-like cells. Accordingly, some tumors had little evidence of lineage differentiation (fig. S13). Furthermore, knockout of the OPC lineage factor *PDGFRA* by use of CRISPR/Cas9 reduced viability in two models of H3K27M-glioma (fig. S15). Combined targeting of *PDGFRA* and the PRC1 subunit *BMI1* further reduced viability of these models (fig. S15). Thus, OPC-like cells are the predominant subpopulation of H3K27M tumors, propagate the disease in patients, and may be susceptible to therapeutic strategies that concurrently target lineage-defined (*PDGFRA*) and somatically altered (*BMI1*) cellular programs.

The H3K27M-glioma hierarchy resembles that in IDH-mutant gliomas; both contain a cycling stem-like subpopulation and differentiated subpopulations of OC-like and AC-like cells. However, they differ in the proportions of subpopulations and in the exact set of genes associated with each program (5, 6). We scored malignant cells from both cohorts by the signatures for H3K27M and IDH-mutant gliomas (5, 6). Astrocytic programs were highly similar (Fig. 3, A and B), whereas oligodendrocytic and stem-like programs are largely distinct, with only a small set of shared genes (Fig. 3, C to F). Indeed, H3K27M-specific stem cell genes were expressed highly by OPCs (such as *PDGFRA*), whereas IDH-specific stem cell genes were expressed by NPCs (such as *SOX11*) (Fig. 3, F and G) (5, 6). Additionally, H3K27M-glioma harbored more cycling and undifferentiated cells than IDH-mutant gliomas (Fig. 3H), potentially accounting for their more aggressive behavior.

We next considered how this cellular architecture relates to genetic heterogeneity and tumor evolution. CNV analysis and inference of haplotypes uncovered distinct genetic subclones in two tumors (Fig. 3, I and J, and figs. S16 and S17) (8). Although all cells in BCH869 have lost one copy of chromosome 14, the subclones had different haplotypes, indicating that two distinct events led to loss of alternate chromosome 14 alleles (Fig. 3J). Additionally, certain somatic gene mutations could be assigned to just one of the subclones (Fig. 3K). Use of both CNVs and haplotype frequencies enabled inference of phylogenetic trees (Fig. 3L, fig. S17D, and table S7) (8). Each genetic subclone contained cells spanning a similar diversity of cellular states, although with some variation in their relative proportions (Fig. 3M and fig. S17E). This suggests that distinct genetic subclones share similar developmental hierarchies in H3K27M-glioma.

Next, we profiled 863 single cells from several models derived from BCH869—including patient-derived xenograft (PDX), gliomaspheres (GS), and differentiated glioma cells (DGC) (fig. S18) (15)—and compared them with cells from the corresponding tumor. Cells from the PDX most closely approximated malignant cell states in the primary tumor, whereas each in vitro model recapitulated some, but not all, of these states (Fig. 4, A and B, and fig. S19A). Tumor-initiation capacity was exclusive to cells grown in GS conditions ($n = 8$ of 8 mice) that partially recapitulated the OPC-like state, and was abolished in DGCs that mirrored the AC-like state ($n = 0$ of 8 mice) (Fig. 4C and fig. S19, B and C), supporting the functional relevance of the inferred hierarchies. Last, we identified differentially expressed genes between the primary tumor, PDX, and culture models (Fig. 4D and table S8). A large number of genes were down-regulated in culture models compared with the primary tumor, including glioma-related oncogenes (such as epidermal growth factor receptor), putative stemness genes (such as SOX2, RFX4, and CD133), and PRC2-targets ($P < 10^{-9}$) (10). PRC2 targets were further down-regulated in DGC (compared with GS), along with neurodevelopmental regulators such as SOX6 and SOX10 (Fig. 4D). This highlights the specificities and limitations of each model.

scRNA-seq of primary H3K27M-glioma defines a putative developmental hierarchy and contrasts the underlying stem cell and differentiation programs with other classes of glioma. The findings are consistent with an emerging cancer stem cell model for gliomas in which (i) genetically defined glioma classes, such as IDH-mutant gliomas and H3K27M-glioma, contain different types of stem-like cells; (ii) the fraction of stemlike cells can vary substantially between glioma types—this extends the traditional cancer stem cell model, which posits that stem cells represent a minority of malignant cells; (iii) differentiation hierarchies play a critical role in the functional properties of glioma cells because self-renewal and tumor-propagating potential are exclusive to the most primitive cells; and (iv) genetic subclones in tumors tend to share similar cellular architecture. Our study also highlights opportunities for therapeutic intervention. We show that OPC-like cells drive H3K27M-glioma, suggesting that the OPC marker PDGFRA could be a lineage-defined therapeutic target, relevant even in the absence of genetic amplification or mutation. H3K27M-glioma also overexpress the PRC1 subunit BMI1 and are sensitive to its inhibition, either alone or in combination with PDGFRA inhibition, hinting at a potential compensatory mechanism for PRC2 dysfunction (Fig. 4E). Thus, lineage-defined and somatically altered cellular programs in H3K27M-glioma suggest complementary opportunities for therapeutic intervention in these incurable malignancies.

Supplementary Material

Refer to Web version on PubMed Central for supplementary material.

Acknowledgments

We thank L. Gaffney for assistance with figures.

Funding: This work was supported by grants from the Alex Lemonade Stand (M.M. and M.L.Su.), the Wang Family Fund (M.L.Su., A.R., B.E.B., and M.M.), the Smith Family Foundation (M.L.Su.), the Broad Institute Broad*next10* (M.L.Su. and O.R.-R.), the V Foundation for Cancer Research (M.L.Su.), the Howard Goodman Fellowship at Massachussetts General Hospital (MGH) (M.L.Su.), the Merkin Institute Fellowship at the Broad

Institute of MIT and Harvard (M.L.Su.), the Rachel Molly Markoff Foundation (M.L.Su. and B.E.B.), NIH–National Cancer Institute (NCI) brain cancer SPORE P50CA165962 (M.G.F., T.T.B., and M.L.Su.), start-up funds from the MGH department of Pathology, The Cure Starts Now Foundation, Hope for Caroline Foundation, Julian Boivin Courage for Cures Foundation, Abbie's Army, Michael Mosier Defeat DIPG Foundation, Reflections of Grace Foundation, The Cure Starts Now Australia, Brooke Healey Foundation, Soar With Grace Foundation, Jeffrey Thomas Hayden Foundation, Cure Brain Cancer Foundation, The Jones Family Foundation, Musella Foundation, Pray, Hope Believe Foundation, Smiles for Sophie Foundation, Benny's World, Love Chloe Foundation, Aiden's Avengers, A Cure from Caleb Society, The Operation Grace White Foundation, Ryan's Hope, Wayland Villars DIPG Foundation, American Childhood Cancer Organization, Juliana Rose Donnelly Trust, Sheila Jones & Friends, The Ellie Kavalieros DIPG Research Fund, Voices Against Brain Cancer, The DIPG Collaborative, Zach Carson Foundation, the Micky Czech Foundation, The Guglietti Family Trust, Prayers From Maria Foundation, Ryan Harvey Foundation, Markoff Art in Giving, and the Brock Fleming Foundation. M.G.F. holds a Career Award for Medical Scientist from Burroughs Wellcome Fund and K12 Paul Calabresi Career Award for Clinical Oncology–Training Program in Nervous System Tumors (K12CA090354). I.T. was supported by the Zuckerman STEM Leadership Program and the Benoziyo Endowment Fund for the Advancement of Science. V.H. was supported by a European Molecular Biology Organization long-term fellowship and a Human Frontier Science Program fellowship. C.N. is supported by the Placide Nicod Foundation. K.L.L., L.G., and M.W.K. received support from NCI grant P01 CA142536. K.E. is supported by the Fondation Nuovo-Soldati. P.B. and R.B were supported by the St. Baldrick's Foundation, the Pediatric Brain Tumor Foundation, Gray Matters Brain Cancer Foundation Olivia Caldwell Foundation, and NCI (grants R01CA219943 and R01CA188228). A.R. was supported by funds from the Howard Hughes Medical Institute, the Klarman Cell Observatory, STARR cancer consortium, NCI grant 1U24CA180922, NCI grant R33CA202820, by the Koch Institute Support (core) grant P30-CA14051 from NCI, the Ludwig Center, and the Broad Institute. B.E.B. was supported by the NIH Common Fund and National Cancer Institute (grant DP1CA216873), the American Cancer Society, the Ludwig Center at Harvard Medical School, and the Bernard and Mildred Kayden MGH Research Institute Chair. Flow cytometry and sorting services were supported by shared instrumentation grant 1S10RR023440-01A1. M.M. was supported by the California Institute of Regenerative Medicine (CIRM) grants RB4-06093 and RN3-06510, Lyla Nsouli Foundation, and the Virginia and D. K. Ludwig Fund for Cancer Research. C.L., A.M.C., and J.M. are supported by The Alicia Pueyo Foundation.

References

1. Sturm D, et al. Nat. Rev. Cancer. 2014; 14:92–107. [PubMed: 24457416]
2. Funato K, Major T, Lewis PW, Allis CD, Tabar V. Science. 2014; 346:1529–1533. [PubMed: 25525250]
3. Lewis PW, et al. Science. 2013; 340:857–861. [PubMed: 23539183]
4. Patel AP, et al. Science. 2014; 344:1396–1401. [PubMed: 24925914]
5. Tirosh I, et al. Nature. 2016; 539:309–313. [PubMed: 27806376]
6. Venteicher AS, et al. Science. 2017; 355:eaai8478. [PubMed: 28360267]
7. Picelli S, et al. Nat Protoc. 2014; 9:171–181. [PubMed: 24385147]
8. Material and methods are available as supplementary materials.
9. Liau BB, et al. Cell Stem Cell. 2017; 20:233–246.e7. [PubMed: 27989769]
10. Ben-Porath I, et al. Nat. Genet. 2008; 40:499–507. [PubMed: 18443585]
11. Darmanis S, et al. Cell Reports. 2017; 21:1399–1410. [PubMed: 29091775]
12. Kreso A, et al. Nat. Med. 2014; 20:29–36. [PubMed: 24292392]
13. La Manno G, et al. Cell. 2016; 167:566–580.e19. [PubMed: 27716510]
14. Marques S, et al. Science. 2016; 352:1326–1329. [PubMed: 27284195]
15. Suvà ML, et al. Cell. 2014; 157:580–594. [PubMed: 24726434]

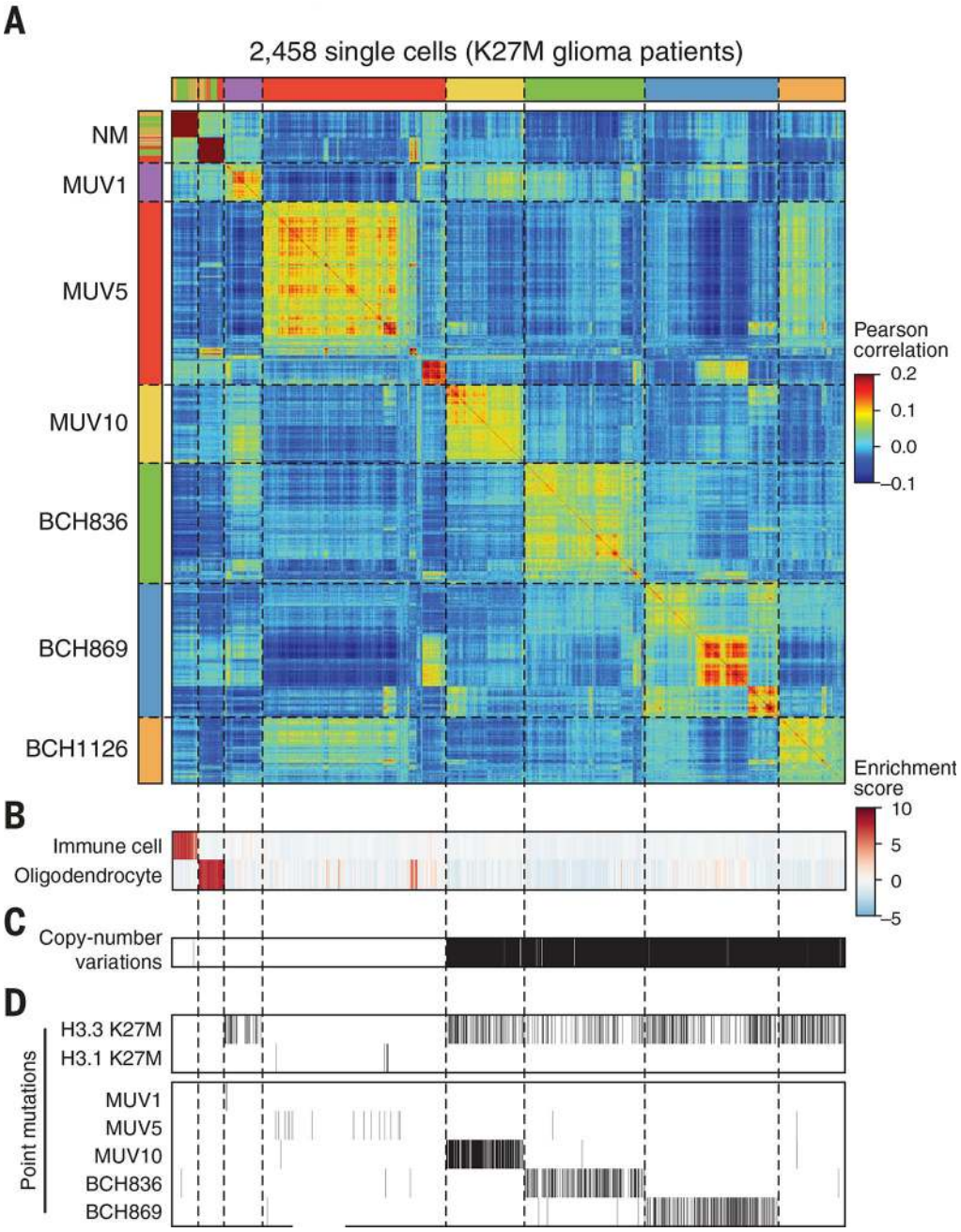

Fig. 1. Characterization of H3K27M-glioma by means of scRNA-seq

(**A**) Pairwise correlations between the expression profiles of 2458 single cells (rows, column) from six H3K27M-glioma samples (color bar). Two clusters of nonmalignant cells are marked as "NM." (**B**) Enrichment score of microglia and oligodendrocyte signatures. (**C**) Inferred CNV profiles. Black indicates CNV present (fig. S4). (**D**) Gene mutations. (Top) H3K27M.; (Bottom) All other mutations identified per sample by means of WGS/WES. Black line indicates at least one mutated gene identified (fig. S6).

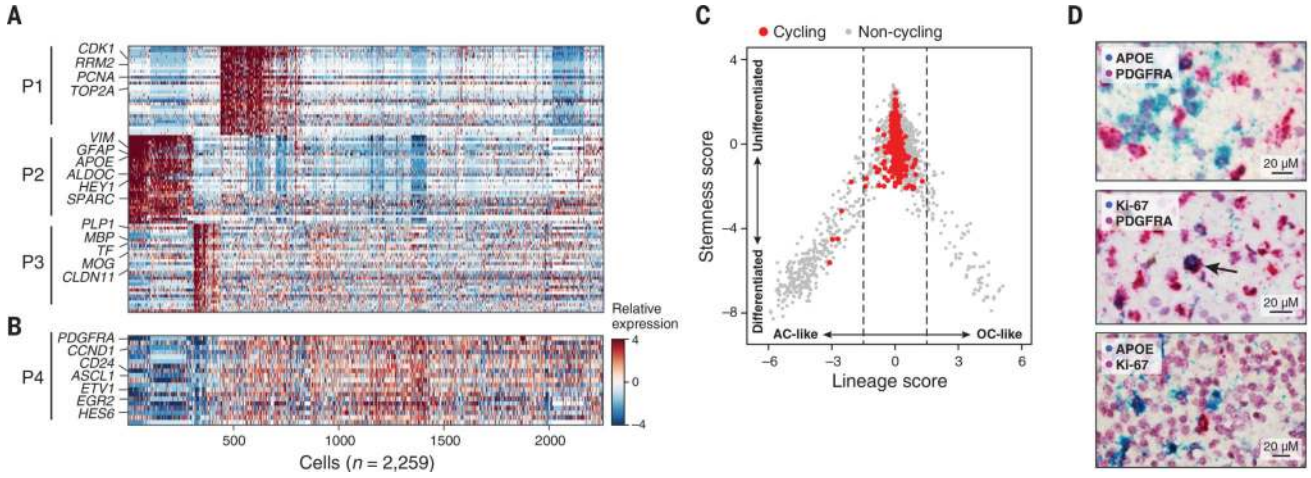

Fig. 2. Intratumor heterogeneity in H3K27M-glioma

(**A** and **B**) Relative expression (color bar) across 2259 malignant cells (columns) of the top 30 genes for each of the combined expression programs P1, P2, and P3 [(A), rows] or 19 genes [(B), P4] that are preferentially expressed in cells with low expression of P1, P2, and P3 (8). (**C**) Plot of the lineage (*x* axis) and stemness (*y* axis) scores for each of 2259 malignant cells (dots). Red dots indicate positive score for the cell cycle program. (**D**) In situ RNA hybridization of H3K27M glioma for astrocytic-like (*APOE*), OPC-like (*PDGFRA*), and proliferation (*Ki-67*) markers. Arrow highlights cell coexpressing *PDGFRA* and *Ki-67*.

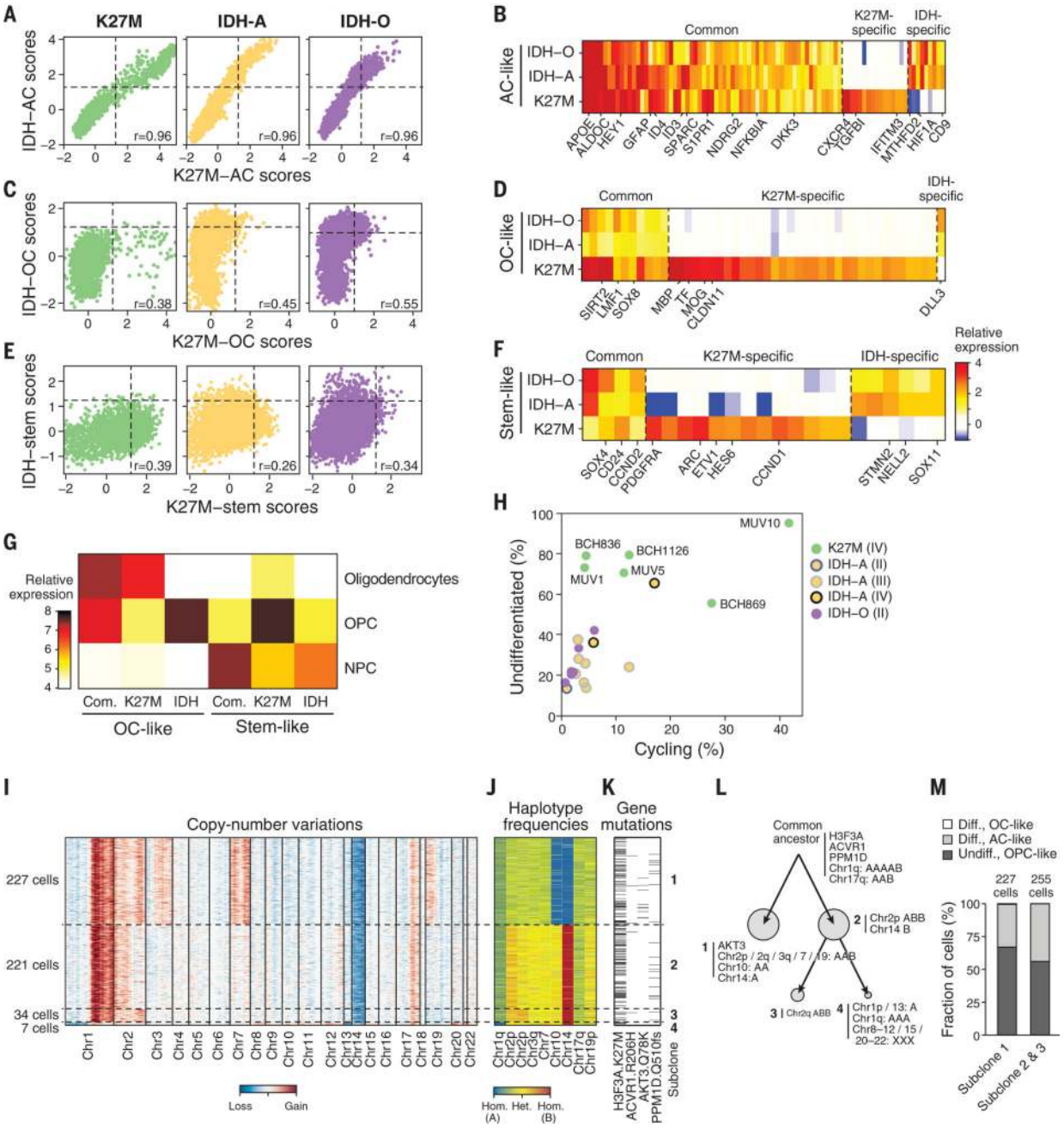

Fig. 3. Cellular hierarchies of H3K27M-glioma and IDH-mutant gliomas

(**A, C**, and **E**) Malignant cells (dots) from H3K27M, IDH-A, and IDH-O scored for the (A) AC-like, (C) OC-like, and (E) stem-like signatures of H3K27M-glioma (*x* axis) and of IDH-mutant gliomas (*y* axis). Correlation values are in the bottom right quadrant. (**B**, **D**, and **F**) Relative expression in (B) AC-like, (D) OC-like, and (F) stem-like cells in each glioma class (rows) of genes with preferential expression in the respective cell subset (8), with genes ordered into those common to H3K27M and IDH-mutant gliomas, or specific to either tumor type. (**G**) Relative expression (color bar) of OC-like and stem-like genes shared between (common) or specific to H3K27M and IDH-mutant gliomas in nonmalignant

oligodendrocytes, OPCs, and NPCs (5). (**H**) Percentage of cycling cells (*x* axis) and undifferentiated cells (*y* axis) in each glioma sample, marked by type and grade. (**I**)CNVs, (**J**) haplotype frequencies, and (**K**) point mutations in selected genes identified with WGS (columns) inferred for individual malignant cells (rows) from BCH869. Dashed lines indicate four subclones based on CNV and haplotype profiles. (**L**) Inferred phylogenetic tree (8) of individual subclones detected for BCH869. Circle sizes indicate relative number of cells in subclone. Genetic events are indicated at the inferred point of their first detection. (**M**) Relative number of malignant cells classified into OPC-, AC-, or OC-like states for BCH869 subclone 1 or the combination of subclones 2 and 3.

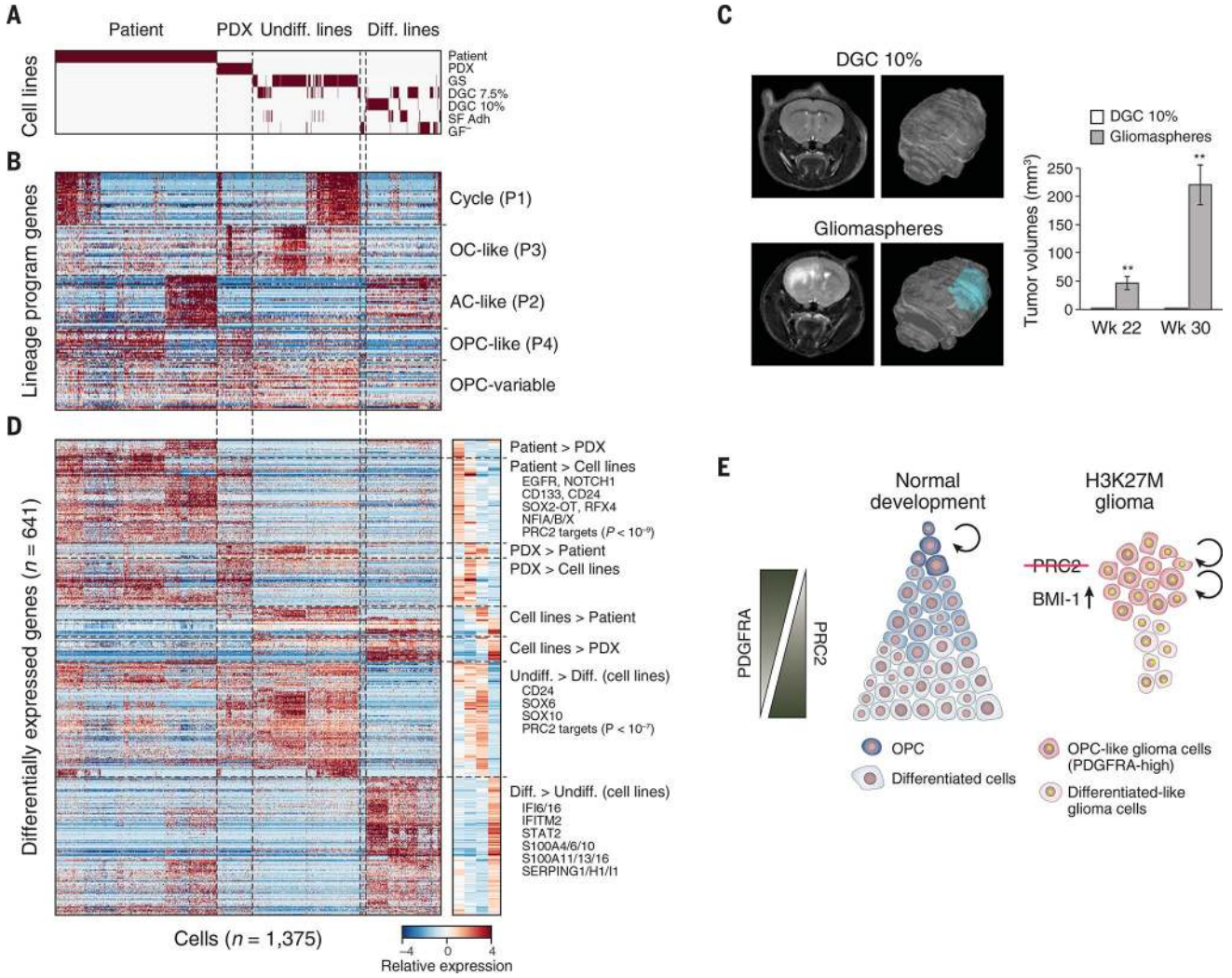

Fig. 4. Single-cell comparisons of matched H3K27M-glioma patient sample, PDX, and culture models for tumor BCH869

(**A**) Cells ordered by sample type and within each sample by means of hierarchical clustering (fig. S19). (**B**) Heatmap shows expression of the top 30 genes of the cell cycle and lineage programs (P1 to P4) described in Fig. 2 and in (8), for cells ordered as in (A). (**C**) (Left) Mouse brain magnetic resonance images (MRIs) with three-dimensional reconstruction at 22 weeks after injection of 200,000 BCH869 cells. (Right) MRI tumor volume (8). $^{**}P < 0.01$ by paired, two-tailed Student's *t* test. Error bars indicate SEM. (**D**) Heatmap shows expression of differentially expressed genes between sample types, for each pairwise comparison. Cells are ordered as in (A). (Right) Average expression in each sample type. (**E**) Model of H3K27M-glioma cellular architecture (right) compared with normal development (left).